ICAS 2021 SHANGHAI
International Council of the Aeronautical Sciences
32nd Congress of the International Council of the Aeronautical Sciences
September 6-10, 2021
Pudong Shangri-La, Shanghai, China

THEORETICAL AND EXPERIMENTAL INVESTIGATION OF THE AEROELASTIC CHARACTERISTICS OF THE AFLONEXT PROJECT BIG-SIZE DEMONSTRATOR

G.A. Amiryants[1], A.V. Chedrik[1], V.A. Malyutin[1] , S.E. Paryshev[1], V.G. Soudakov[1]

[1] Central Aerohydrodynamic Institute (TsAGI), Zhukovsky, Russia

Abstract

AFLoNext is an integrated project of the 7th European Framework Programme of the EU with the objective of proving and maturing highly promising flow control technologies for novel aircraft configurations to achieve quantum leap in improving aircraft's performance and, thus, reducing the environmental footprint.

Active Flow Control (AFC) on airframe targets to show the net benefit of integrated AFC for understanding of the functionality of AFC and its application on a sensitive airframe region. Furthermore, the aim of this work package is to overcome the problem by actively suppressing local flow separation linked to the wing/pylon junction by means of AFC through energizing the flow with fluidic jets. The aim of the activities in which TsAGI is mainly involved is to prove the Technology Readiness Level (TRL) 4 for the AFC at the Engine-Wing junction.

The main steps prior to Wind Tunnel (WT) tests were design and manufacturing of large-scale WT model that is suitable for representation of typical flow separation phenomena near the junction of Ultra High Bypass Ratio (UHBR) engine with the wing. The use of UHBR engines is currently one of the most promising approaches for further increase of the efficiency of classical transport aircraft configurations. The UHBR engines appropriately can be mounted under swept wings to increase aerodynamic efficiency. The close coupling of large nacelles and the wing deteriorates the mounting of leading edge high lift devices such as slats, Krueger flaps or droop noses over a large part of the wing in the area of the engine-wing junction. For high angles of attack local flow separation regions are emerging on the wing suction side in the wake of the nacelle, which are called nacelle-wake separation. This flow separation should be obtained in WT tests at low speed and it can trigger total wing stall which degrades total aircraft performance. To avoid this phenomenon two types of AFC technologies for high-lift configuration were investigated: the pulsed jet actuator (PJA) and the synthetic jet actuator (SJA). These technologies were tested on a large-scale demonstrator under realistic flow conditions and with flow control systems representative for future flight tests. The large-scale wind tunnel tests were performed at the facility WT-101 of TsAGI.

Overall objective of the presented activity is:

– Refinement of the developed FEM on the basis of ground vibration tests (GVT) and stiffness measurements (SM) results;

– Providing safety of the demonstrator WT tests against flutter and divergence conditions;

– Refinement of WT tests results on the basis of installation estimations and direct measurements of local angles of attack (AoA) increment in spanwise direction of the wing demonstrator due to its elastic deformations.

Keywords: static aeroelasticity, flutter, structural elastic deformations, wing flow control

1. Introduction

A promising problem of modern aerodynamics of passenger aircraft is to improve their aerodynamic characteristics. New approaches to solve the problem widely use optimization procedures to find the best solutions within the conventional techniques in aerodynamics. At the same time, the further significant increase in the lift-to-drag ratio of aircraft is difficult. One of the most essential and innovative ways to improve aerodynamic characteristics is using aircraft flow control. This work investigates a promising scientific field, i.e. boundary layer control.

The aim of the project under consideration of the 7th European AFLoNext Framework Program is to develop advanced flow control technologies for new aircraft configurations with the objective of significant improvement of aerodynamic characteristics and reduction of negative environmental impact.

In this paper, experimental studies of two innovative boundary layer control systems are performed in the wind tunnel WT-101 on a large-scale demonstrator of a passenger aircraft. These systems are created under the leadership of Airbus Innovation Group and Fraunhofer:

– blowing of jets from a special nozzle on the upper surface of the wing by using a pulsed jet actuator (pulsed jet actuator – PJA, developed by Airbus) [1–3],

– the system of synthetic jets (the flow gets impulse by means of vibrating membranes without blowing mass), created by use of synthetic jet actuators (synthetic jet actuator – SJA proposed by the Fraunhofer in cooperation with NLR) [4, 5]

This study aims to find advanced opportunities to increase aerodynamic characteristics of the aircraft wing at take-off and landing regimes. It required to solve the specific multi-directed task of developing and testing WT flow systems that ensure robustness of these boundary layer control systems proposed by TsAGI partners.

The work on the design, development and manufacture of the corresponding demonstrator was complicated by the need to perform various complex measurements on it during the tests in the WT-101. In particular, tests included measurement of steady pressure on the demonstrator wing; balance measurements; measurement of mass airflow consumption in the boundary layer control system; visualization of the flow around the wing using colored particles and mini-strips; measurements of deformations of the model elements; determination of dynamic stability characteristics of the demonstrator in the wind tunnel flow.

In order to eliminate undesirable phenomenon of flow separation on the wing at low flight speeds and high angles of attack, due to the presence of a large engine nacelle, the project explores two of these types of technologies for active flow control on wings with high lift-to-drag ratio. These promising technologies have been studied on a large-scale demonstrator in the TsAGI WT-101. It is built on the basis of the SADE project demonstrator with an unswept "clean" (without engine) wing [6]. The goal of the SADE (SmArt High Lift DEvices for Next Generation Wings – the European 7th Framework Program) project was to study the "smart" elements of the mechanization of next-generation wings. To study the aeroelasticity and strength problems of the SADE demonstrator, we used approaches based on the Nastran software. The experimental methods used for non-contact measurements of deformations are based on the papers [7-10].

2. Some aspects of the demonstrator mathematical model development

The main purpose of this work was to develop a mathematical model of the AFLoNext project demonstrator for strength analysis, to provide safe tests in the WT-101 under the conditions of aeroelasticity, and to ensure that the influence of elastic deformations on the aerodynamic characteristics of the demonstrator during take-off and landing flight regimes is taken into account.

A general view of the demonstrator structure is shown in Fig. 1 (left). On the right is a diagram of the components.

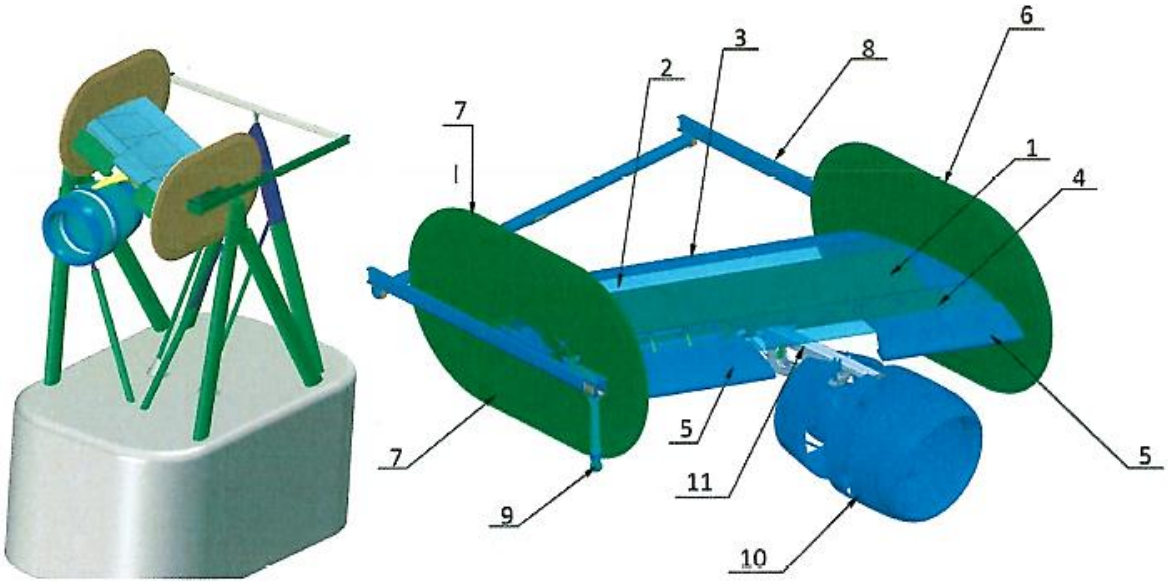

Figure 1 – General model view (left) and model component scheme (right)

1 – Wing-box, 2 – Trailing edge, 3 – Flap, 4 – Leading edge, 6,7 – End-plates, 8 – Model support on the wind tunnel mechanical balance, 9 – Compressed air supply system, 10 – Engine Nacelle, 11 – Engine Nacelle Pylon.

The wing compartment in the area of the engine nacelle attachment has the following main sizes: the sweep angle along the leading edge is 28°, the span is 5.96 m, the chord length is 3.259 m, the wing area is 16.29 m2. The range of the studied angles of attack during the tests is 10-31°, and the range of the studied flow velocities is 20-50 m/s.

The model components marked by numbers in Fig. 1 were separate zones, according to which the inertial characteristics of the structure were identified.

The geometric CAD model of the demonstrator was prepared in the CATIA system. The AFLoNext project demonstrator includes both elements of the SADE project demonstrator (wing box, end-plates) and new components (engine nacelle with internal body, pylon, leading and trailing edges, slat and flap). The CAD model was imported into the MSC.Nastran, in which a refined thin-walled finite element model containing shell and beam elements was generated. The total number of elements in the model was 106320, and the total number of nodes was 79637 (Figure 2).

In Fig. 2, the boundary conditions of the demonstrator are shown in red color. The vertical supports in the tests have a hinged attachment to the WT-101 mechanical balance, so the translational degrees of freedom were fixed in their bottom nodes. The nodal translational degrees of freedom in the vertical and lateral directions and the rotational degree around the vertical axis were fixed on the horizontal beam of the support device at the joint area.

The pink color corresponds to the elements representing the attachment of leading and trailing edges to the wing-box, the pylon to the engine nacelle and the wing-box.

The demonstrator's structural parts were made of different materials, namely: steel, aluminum alloys, obomodulan, and wood.

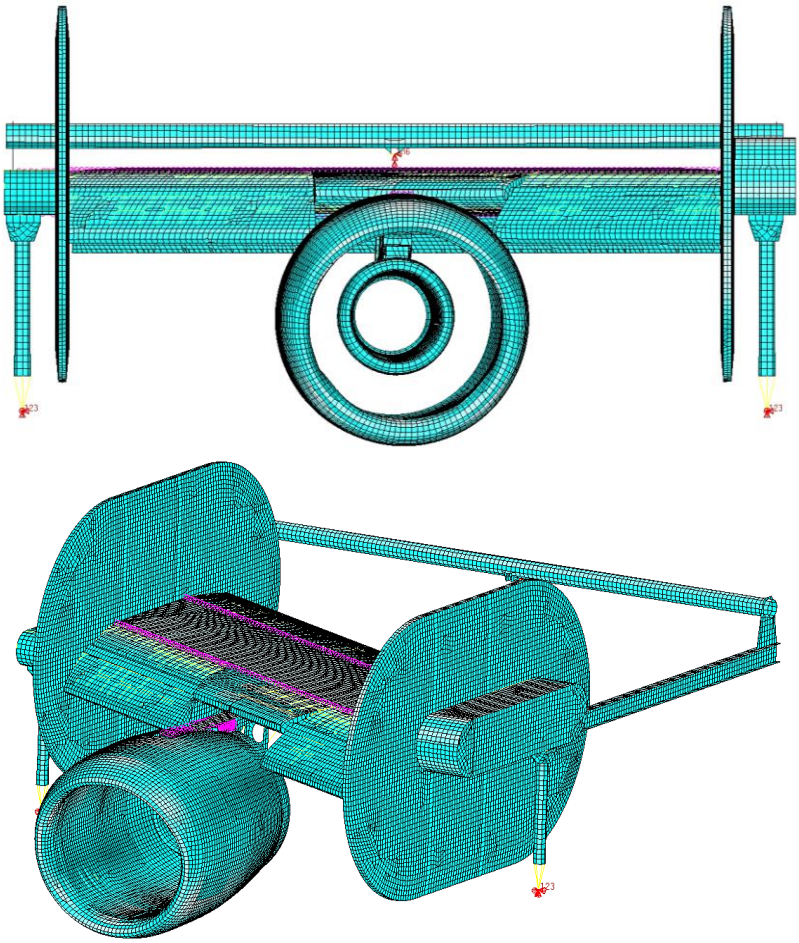

Figure 2 – FE model of the demonstrator in frontal (top) and isometric (bottom) views.

Main geometric parameters of structural elements, such as thickness of the skin and cross-sections of beam elements, were transferred as precisely as possible from the geometric to the finite element model. Nevertheless, a sufficiently accurate transfer of dimensions ensures the correct reproduction only of stiffness characteristics. In fact, any design has "non-structural elements" and elements that cannot be included in the global analysis model. Therefore, it is necessary to identify the structure by both stiffness and mass characteristics. Since there were no experimentally measured stiffness characteristics, the identification was carried out only by the weights and gravitational centers for the above-mentioned structural components.

The identification was to approximate the masses of the analysis model to the masses obtained by weighing the components of the real demonstrator model. The problem was that the non-structural mass added to the mathematical model should not increase the structural stiffness. An applied intuitive approach was concluded in adding non-structural mass to ensure the weight balance and the components' gravity center positions.

3. Analysis of stresses and strains

Before testing the demonstrator in the WT-101 flow, the displacement and equivalent stresses under influence of structural weight were calculated using the developed design model for two positions of the demonstrator: at zero angle of attack and an angle of attack equal to 30°. The results showed that the maximum deflections of the demonstrator under gravitational load at zero angle of attack were seen at the leading edge of the external contour of the engine nacelle and were 3 cm. In the case of the demonstrator directed at an angle of 30°, the maximum deformations were located in the trailing part of the right end-plate and were equal to 6 cm. With the wing demonstrator being directed at an angle of attack of 30°, the highest stresses were located in the right part of the attachment of the wing-box to the supporting device and were equal to 120 MPa (the maximum stresses in this zone were σ_T=420 MPa), which corresponded to a safety margin of η=3.5. The Mises stress distribution in the demonstrator design is shown in Fig. 3.

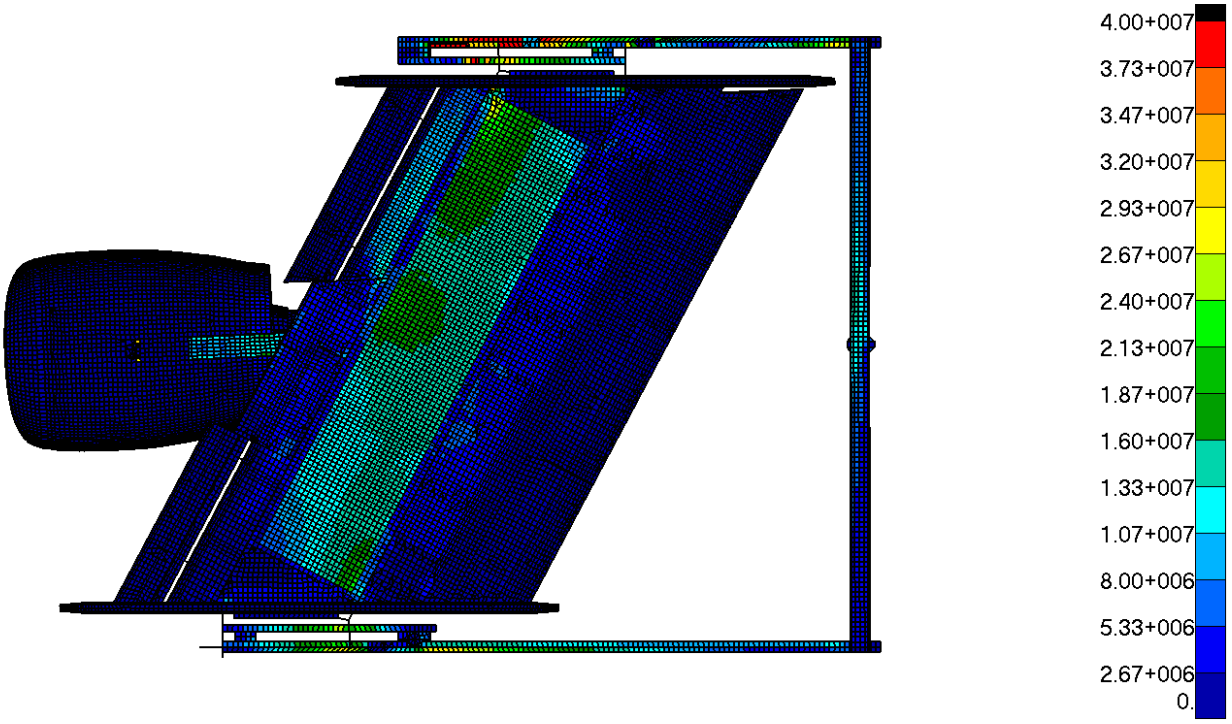

Figure 3 – Mises stress distribution in the demonstrator structure (top view).

Based on calculations without considering the flow effect on the demonstrator, it was decided to strengthen the attachment area of the wing box spar to the support beam that led to a significant stress reduction in this zone.

4. Modal analysis

The modal analysis results for the identified mathematical model of the demonstrator are presented for four modes in Fig. 4.

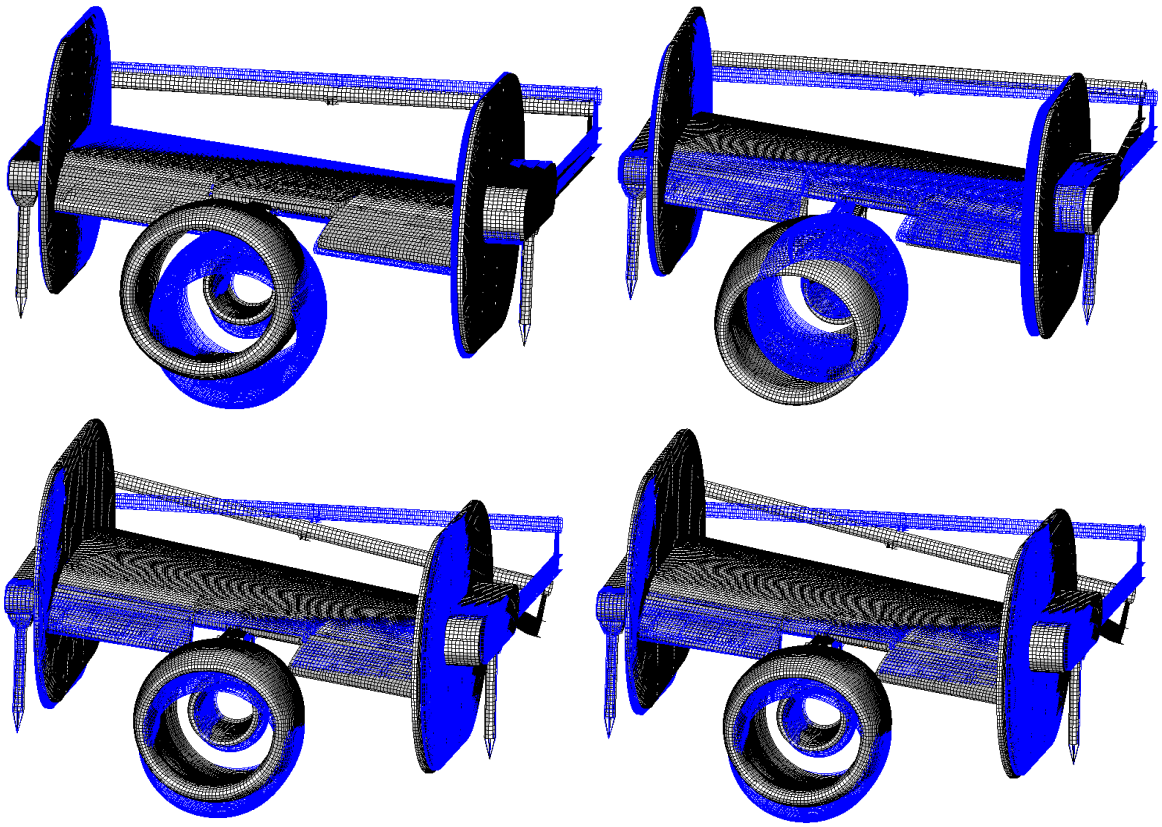

Figure 4 – First natural modes of the demonstrator.

The analysis of the ground vibration test results of the demonstrator wing in the working part of the WT-101 indicates their satisfactory accordance with the result obtained by means of Nastran system. The calculated and experimental values of the natural frequencies of the five lowest modes of the elastically suspended demonstrator were, respectively: the first mode – 3.04 and 2.75 Hz, the second – 4.23 and 3.97 Hz, the third – 4.5 and 4.13 Hz, the fourth – 6.36 and 5.96 Hz, the fifth-9.33 and 8.92 Hz.

5. Limit load factors determination and flutter analysis

To analyze the behavior of the demonstrator structure in the flow an aerodynamic model consisting of aerodynamic panels was generated in the MSC.FlightLoads system (Figure 5).

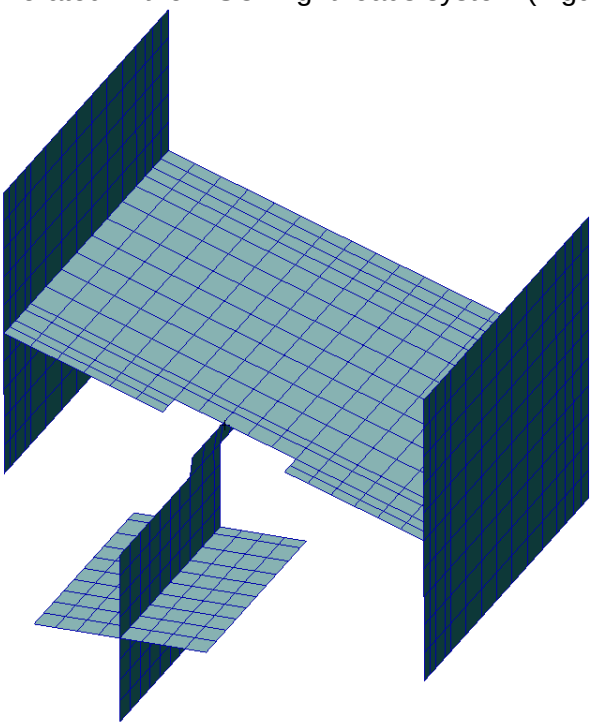

Figure 5 – Aerodynamic model of the demonstrator.

The calculation of loads on the aerodynamic model was carried out using the doublet lattices method, implemented in the software package MSC. Nastran. The interaction of the dynamically scaled model with the aerodynamic model was reproduced by virtue of the SPLINE4 element. The demonstrator strength analysis under the influence of maximum aerodynamic loads (the installation angle of the demonstrator α=30°, the flow rate V=50 m/s) showed that the weakest elements are the bracing of the pylon attachment to the wing box, the brackets of the slat attachment and the beams of the supporting device.

The minimum margin of safety in the most loaded structural elements was at least η=3, which corresponds to the requirements of WT-101. However, the presence of flow turbulence and "disruptive" phenomena could reduce this margin. Therefore, during the start-up process, in order to control the vibrations of the engine nacelle and slat, vibrations were monitored using in-model load factor sensors, for each of which the maximum load factor value was determined and specified calculated from the minimum admissible safety margin η=2. The maximum load factor values for the *i*-th mode were determined from the ratio:

$$N_{max}^{i} = 4\pi^2 \nu_i^2 \left| z_{max}^{i} \right| / g,$$

where ν_i is the natural frequencies of the demonstrator structure, z_{max}^{i} is the limit amplitudes of the structure in the sensor location for given modes, and *g* is the gravitational acceleration.

The limit amplitude was determined from the analysis of dynamic stresses in the MSC. Nastran system as follows:

$$z_{\max}^{i} = z_0^{i} \frac{\sigma_{\text{dyn max}}^{i}}{\sigma_{\text{dyn adm}}^{i}},$$

where z_0^i is the amplitude of vibrations in the sensor, $\sigma^i_{\text{dyn max}}$ is the maximum dynamic stress in the structural element for the *i*-th mode, the maximum admissible dynamic stress in this structural element is $\sigma^i_{\text{dyn adm}} = \frac{\sigma^i_{\text{adm}}}{\eta} - \sigma^i_{\text{stat}}$, determined by the limit stress of the material σ^i_{adm} and the static stress σ^i_{stat} with the value of the safety margin – η.

Load factor sensors' location used to monitor the dynamic state is shown in Fig. 6. Sensor #2 measures the load factor N_y, the other sensors – N_z.

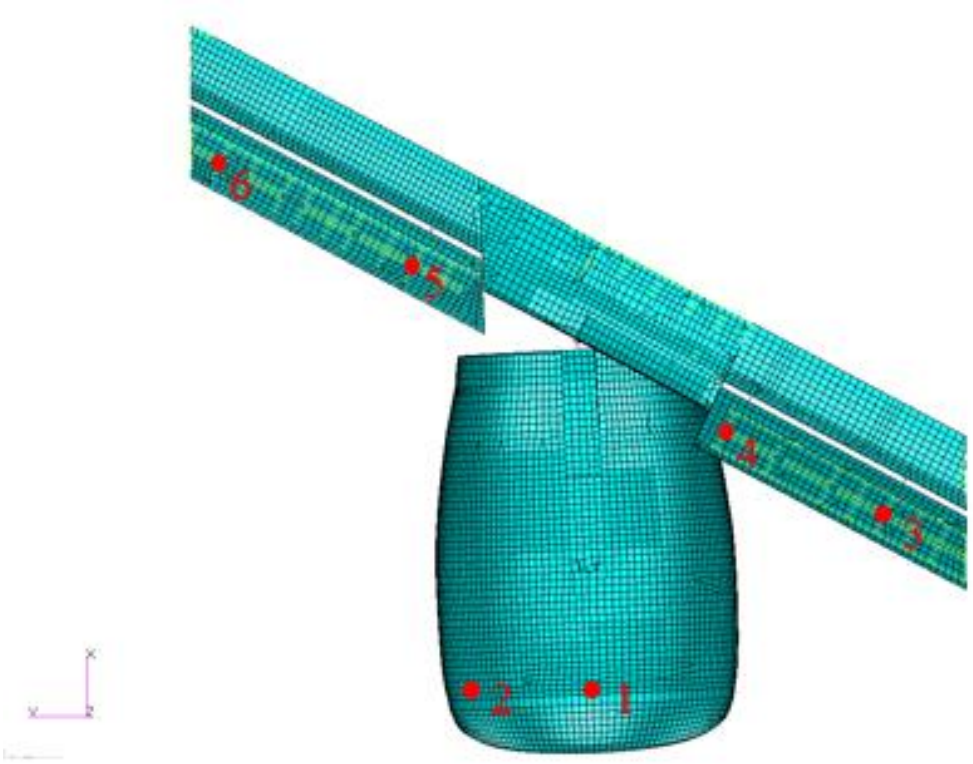

Figure 6 –Location of load factor sensors.

The maximum load factor values are determined for the first several modes with high amplitudes in each sensor zone with a safety factor η=2 and are shown in Table 2.

Before wind tunnel runs, the critical flutter velocity was determined in the MSC.Nastran system. The aerodynamic model was used to determine the critical flutter velocity. The following load case was considered: Mach number *M*=0.15, the range of Strouhal numbers *Sh*=0.01, 0.5, 1.0, 2.5, 5.0, 7.5, 10.0, air density ρ =1.225 kg/m^3, speed range 1–400 m/s. Computational studies of the demonstrator mathematical model showed absence of flutter and divergence within the operating range of flow speeds in the WT-101. According to the calculation, the critical divergence velocity was 285 m/s (at this speed, the frequency of the first mode decreases to 0 Hz), and the critical flutter velocity was 342 m/s (the interaction of the 8th and 9th engine modes). A *v-g* diagram representing the dependence of the logarithmic decrement and structural natural frequencies on the speed is shown in Fig. 7. It is considered that the flutter occurs when the logarithmic decrement becomes negative. In this case, the considered mode approaches the neighboring one by frequency. At the divergence, the frequency of the mode tends to zero, and the logarithmic decrement tends to negative infinity.

	f, Hz	$N_{z\,max}$	$N_{y\,max}$		f, Hz	$N_{z\,max}$	$N_{y\,max}$		f, Hz	$N_{z\,max}$	$N_{y\,max}$
Sensor 1	1.87	0.64	–	Sensor 2	1.39	–	0.29	Sensor 3	3.21	0.35	–
	2.86	0.27	–		2.86	–	0.68		7.04	1.29	–
	3.21	1.33	–		3.51	–	0.53		10.35	3.56	–
	3.51	0.73	–		10.35	–	10.87		10.73	2.7	–
	5.62	2.13	–		10.73	–	5.14		18.65	6.05	–
	7.04	0.8	–						24.18	6.92	–
									49.35	29.58	–
Sensor 4	7.04	1.13	–	Sensor 5	7.04	0.67	–	Sensor 6	18.65	11.15	–
	10.73	2.34	–		18.65	12.19	–		19.1	4.86	–
	24.18	5.89	–		19.1	5.63	–		24.18	3.98	–
	49.35	22.53	–		24.18	3.94	–		27.33	18.82	–
					27.33	12.07	–				
					35.91	19.93	–				

Table 2 – Maximum load factor values in sensors.

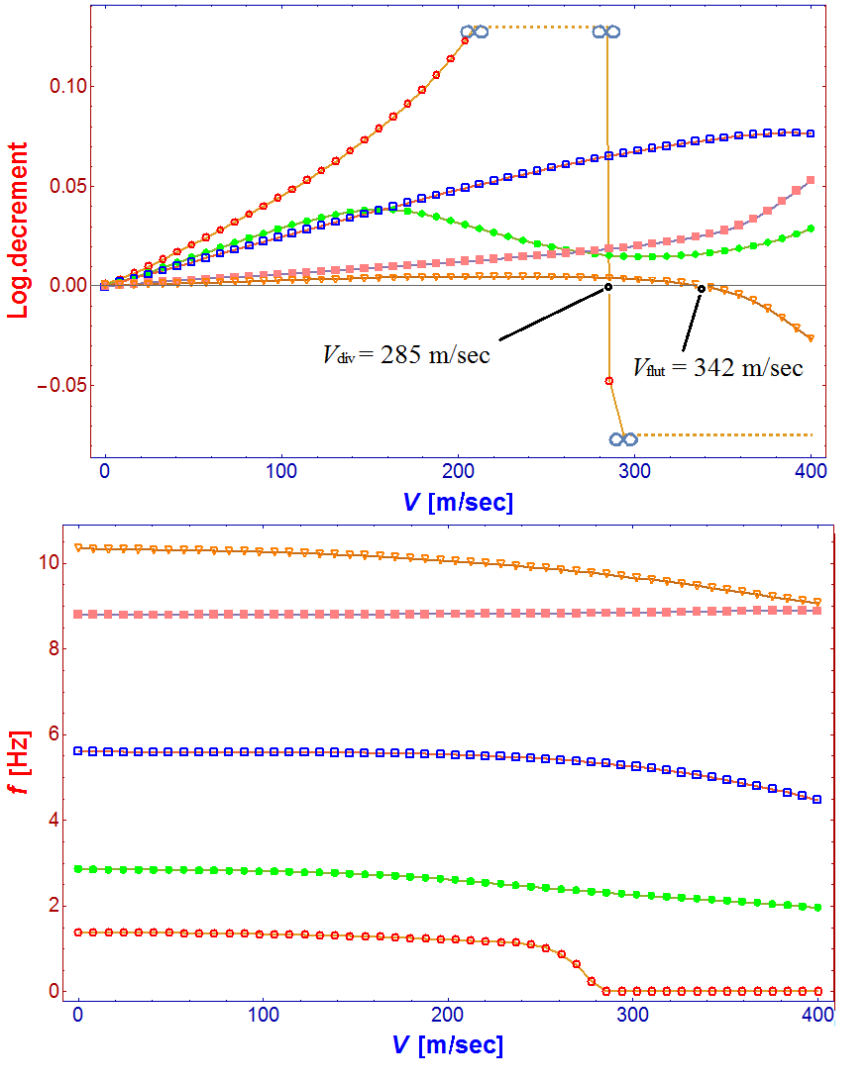

Figure 7 – The *v-g* diagram for the AFLoNext demonstrator.

Based on the calculated data, the demonstrator was allowed to be tested according to the test program, providing that the actual aerodynamic loads (obtained after the first run) were not more than 10 % higher than the calculated ones.

6. Comparison of experimental and calculated increments of the demonstrator local angles of attack

In the WT-101 flow, the local angles of attack of the model elements were measured using in-model angular displacement sensors. Small-sized sensors based on two-axial micromechanical accelerometers were used as angular displacement sensors.

Metrological characteristics of the sensors were determined during the calibration process comparing with the reference value in the range of angles from –30° to 30°. On average, the confidence errors of the sensors (taking into account the mutual influence of both channels) on the angle of attack channel in the range of local angles realized during the tests did not exceed 0.05°. However, since the temperature dependence of the sensor readings and the influence of vibrations have not been studied (other reasons for errors are possible), a value of 0.1°can be taken as the error in measuring the angles of attack.

The locations of the sensors are shown in Fig. 8. The sensitivity axes of all sensors were directed in the same way: the *X*-axis – in the positive direction of the OX axis (backward to the flow), the *Y*-axis – in the negative direction of the OZ axis (Figure 8).

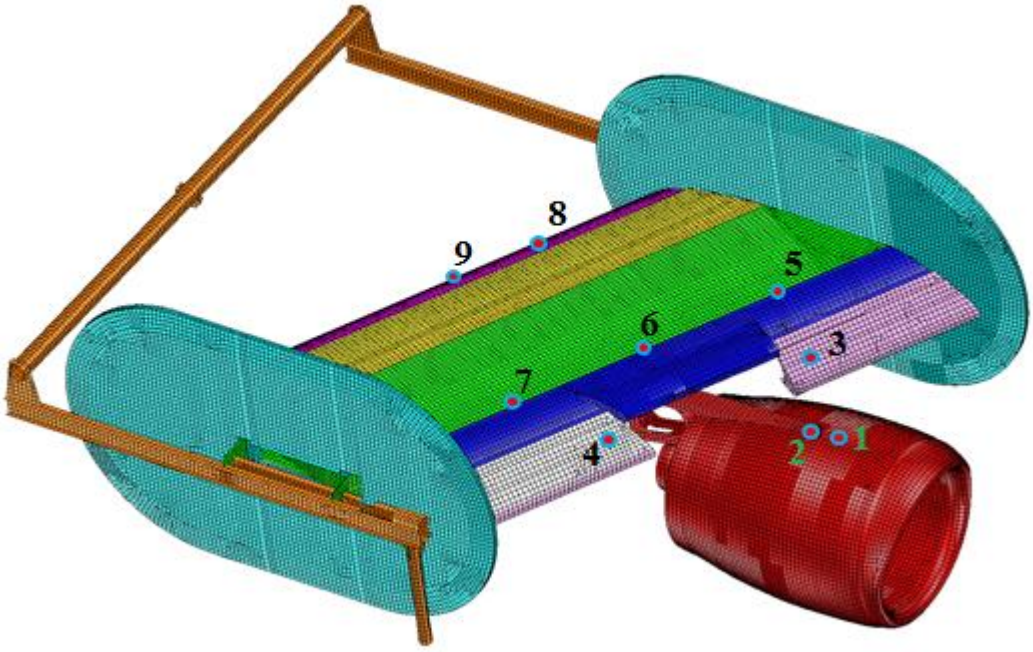

Figure 8 – The FEM of the demonstrator with AoA sensor positions.

The variation of roll angles and local angles of attack from the change of the gravity vector direction at condition without airflow was not detected (did not exceed the error of sensors). Therefore, only the change of local attack angles from the airflow influence was studied and calculated from the difference between corresponding angles without/with the airflow.

Comparison of experimental and calculated angles of attack was carried out for the angles of the demonstrator installation in the flow α=20°, 30° and the flow velocity V_{flow}=20, 30, 40 and 50 m/s. For these cases, the increments of nodal rotational angles at the locations of sensors around the Z-axis (increments in the angle of attack) were determined in the finite element model. In order to avoid local measurement errors, we used a linear approximation of the experimental values for specified attack angles of the demonstrator model.

The comparison of the calculated and experimental results is presented by diagrams in Table 3. In the diagrams, the sensor numbers are marked on the *X*-axis, and the value of the increment of the local attack angle is shown on the *Y*-axis. The red columns indicate the calculated increments of the local angles of attack, and the green columns indicate the corresponding experimental values.

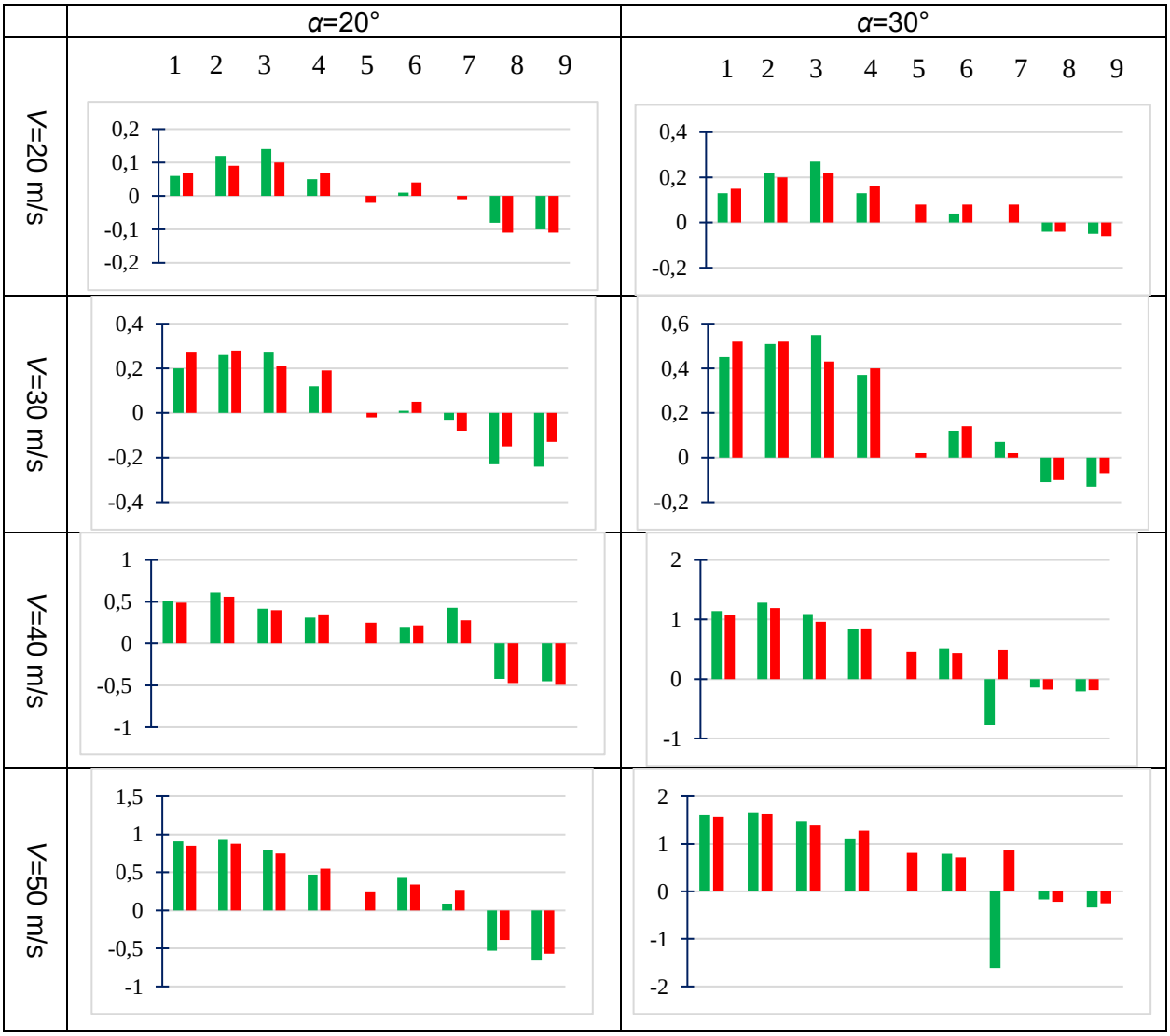

Table 3 – Graphical comparison of calculated and experimental values of increments of local angles of attack in different modes.

As it can be seen, the increment of the demonstrator local angle of attack (due to elastic deformations of structural elements and the change in the flow velocity) is especially significant (more than 1.5°) at an angle of attack of 30° and a flow velocity of 50 m/s in the area of the front joint of the engine pylon. It is also significant (more than 0.7°) in the zone of the front spar of the wing box. The satisfactorily consistent results of the corresponding calculations and experiments were taken into account when analyzing the effectiveness of the two innovative boundary layer control systems studied in the project.

7. Conclusion

Based on the performed computational and experimental research, the strength requirements and dynamic stability of the demonstrator in the WT flow were provided within the 7th European AFLoNext Framework Program. Two types of Active Flow Control (AFC) technologies for high-lift configuration were investigated using this demonstrator: the pulsed jet actuator (PJA) and the synthetic jet actuator (SJA). Another achieved goal was to ensure high accuracy of the measurement efficiency of the wing flow control systems, thanks to the precise accounting of elastic deformations of the demonstrator elements under the influence of gravitational and airflow forces.

8. Acknowledgments

The work described in this paper and the research leading to these results have received funding from the European Community's Seventh Framework Programme FP7/2007-2013, under Grant agreement no. 604013, AFLONEXT project.

9. Contact Author Email Address

mailto: amiryants@mail.ru, stataer@tsagi.ru

10. Copyright Statement

References

[1] Fricke S., Ciobaca V., Kröhnert A.,Wild J., Blesbois O. Active Flow Control Applied at the Engine-Wing Junction // 5th CEAS Air and Space Conference, CEAS Paper 249, Delft, The Netherlands, 2015.

[2] Ciobaca, V., Wild, J., Norman, D.: Numerical Studies of Active Flow Control Applied at the Engine-Wing Junction; In: Advances in Simulation of Wing and Nacelle Stall, Notes on Numerical Fluid Mechanics and Multidisciplinary Desig. Springer International Publ., Cham, Switzerland, 2016, vol. 131, pp 397–411. DOI:10.1007/978-3-319-21127-5.

[3] Schlösser P., Bauer M. Design of a Pulsed Jet Actuator for Separation Control, CEAS Aeronautical Journal (2020) 11:805-812.

[4] Schueller M., Schippers H., Stefes B., Meer T., Wiegel P., Vrochta P., Wallin S., Meyer M. Aerodynamic Design & System Development of SJA for Flow Control at the Engine/Wing junction // 5th CEAS Air & Space Conference in Delft, Netherlands, 7-11 September 2015

[5] Weigel P., Schüller M., Gratias A., Lipowski M. ter Meer T. Design of a Synthetic Jet Actuator for Separation Control, CEAS Aeronautical Journal (2020) 11:813-821.

[6] Amiryants G.A., Kulesh V.P., Malyutin V.A., Chedrik A.V., Aeroelastic Analysis of the Adaptive Wing Wind Tunnel Demonstrator of the SADE Project. 29-th Congress of ICAS, St-Petersburg, 2014.

[7] Kulesh V.P., Fonov S.D. Measurement of parameters of motion and deformation of aircraft model in a wind tunnel by videogrammetry method. // scientific notes of TsAGI, 1998. v.XXIX, №1-2. – pp.165-176.

[8] Lobanov A.N. Photogrammetry. – Nedra. 1984. - 552 p.

[9] Burner A.W., Tianshu Liu. Videogrammetric model deformation measurement technique. // J. of Aircr., 38. 4, pp. 745-754, 2001.

[10] Kulesh V.P. Non-contact measurement of geometrical parameters of shape, motion and deformation of objects in experimental aerodynamics. - Sensors and Systems, № 3. -pp. 22-27, 2004 .